IEEE Access
Multidisciplinary | Rapid Review | Open Access Journal

Received March 23, 2022, accepted April 19, 2022, date of publication April 25, 2022, date of current version May 6, 2022.

Digital Object Identifier 10.1109/ACCESS.2022.3170035

Survey of Exposure to RF Electromagnetic Fields in the Connected Car

GABRIELLA TOGNOLA[1], MARTA BONATO[1], (Student Member, IEEE), MARTINA BENINI[1,2], SAM AERTS[3], SILVIA GALLUCCI[1,2], EMMA CHIARAMELLO[1], (Member, IEEE), SERENA FIOCCHI[1], MARTA PARAZZINI[1], (Member, IEEE), BARBARA M. MASINI[4], (Senior Member, IEEE), WOUT JOSEPH[3], (Senior Member, IEEE), JOE WIART[5], (Senior Member, IEEE), AND PAOLO RAVAZZANI[1], (Member, IEEE)

[1]Istituto di Elettronica e di Ingegneria dell'Informazione e delle Telecomunicazioni (IEIIT), Consiglio Nazionale delle Ricerche, 20133 Milan, Italy
[2]Dipartimento di Elettronica, Informazione e Bioingegneria (DEIB), Politecnico di Milano, 20133 Milan, Italy
[3]Department of Information Technology, IMEC—Ghent University, 9020 Gent, Belgium
[4]Istituto di Elettronica e di Ingegneria dell'Informazione e delle Telecomunicazioni (IEIIT), Consiglio Nazionale delle Ricerche, 40136 Bologna, Italy
[5]Department of Communication and Electronic (COMELEC), Institut Mines-Telecom, 91120 Palaiseau, France

Corresponding author: Gabriella Tognola (gabriella.tognola@ieiit.cnr.it)

This work was supported in part by the French National Research Program for Environmental and Occupational Health of Anses, EXPOAUTO Project 2020/2 RF/05.

ABSTRACT Future vehicles will be increasingly connected to enable new applications and improve safety, traffic efficiency and comfort, through the use of several wireless access technologies, ranging from vehicle-to-everything (V2X) connectivity to automotive radar sensing and Internet of Things (IoT) technologies for intra-car wireless sensor networks. These technologies span the radiofrequency (RF) range, from a few hundred MHz as in intra-car network of sensors to hundreds of GHz as in automotive radars used for in-vehicle occupant detection and advanced driver assistance systems. Vehicle occupants and road users in the vicinity of the connected vehicle are thus daily immersed in a multi-source and multi-band electromagnetic field (EMF) generated by such technologies. This paper is the first comprehensive and specific survey about EMF exposure generated by the whole ensemble of connectivity technologies in cars. For each technology we describe the main characteristics, relevant standards, the application domain, and the typical deployment in modern cars. We then extensively describe the EMF exposure scenarios resulting from such technologies by resuming and comparing the outcomes from past studies on the exposure in the car. Results from past studies suggested that in no case EMF exposure was above the safe limits for the general population. Finally, open challenges for a more realistic characterization of the EMF exposure scenario in the connected car are discussed.

INDEX TERMS Electromagnetic field exposure, intelligent transportation systems, connected vehicle, V2X, advanced driver assistance systems, ADAS, IoT, intra-car wireless connectivity, 5G NR, radar.

NOMENCLATURE

3GPP	3rd Generation Partnership Project
5G-V2X	5G Vehicle-to-Everything
ACC	Adaptive Cruise Control
ADAS	Advanced Driver-Assistance System
AMPS	Advanced Mobile Phone System
BLE	Bluetooth Low Energy
CDMA	Code Division Multiple Access
C-ITS	Cellular-ITS
C-V2X	Cellular-V2X
DSRC	Dedicated Short-Range Communication
ECU	Electronic Control Unit
E-field	Electric field
EIRP	Effective Isotropic Radiated Power
EMF	Electromagnetic Field
ERP	Effective Radiated Power
ETC	Electronic Toll Collection
FDD	Frequency-Division Duplex
FMCW	Frequency-Modulated Continuous Wave
FR1, FR2	Frequency Range 1, Frequency Range 2

The associate editor coordinating the review of this manuscript and approving it for publication was Giovanni Pau.

GSM	Global System for Mobile Communications
H-field	Magnetic field
IoT	Internet of Things
ISM	Industrial, Scientific and Medical
ITS	Intelligent Transport Systems
ITS-G5	Intelligent Transport Systems-G5
LRR	Long Range Radar
LTE-V2X	Long-Term Evolution V2X
MIMO	Multiple Input Multiple Output
NB	Narrow Band
NFC	Near-Field Communication
NR	New Radio
OBU	On-Board Unit
PaaK	Phone as a Key
PEPS	Passive Entry Passive Start
RF	Radio Frequency
RKE	Remote Keyless Entry
RMS	Root Mean Square
RSU	Road-Side Unit
S_{ab}	Absorbed Power Density
SAR	Specific Absorption Rate
SAR_{1g}, SAR_{10g}	Specific Absorption Rate on 1 g / 10 g
SRR	Short-Range Radar
TDD	Time Division Duplex
TPMS	Tire Pressure Monitoring System
UHF	Ultra-High Frequency
UMTS	Universal Mobile Telecommunications Service
Uu	UMTS Terrestrial Radio Access Network to User Equipment
UWB	Ultra-Wide Band
V2I	Vehicle-to-Infrastructure
V2N	Vehicle-to-Network
V2P	Vehicle-to-Pedestrian
V2V	Vehicle-to-Vehicle
V2X	Vehicle-to-Everything
VHF	Very High Frequency
VOD	Vehicle Occupant Detection

I. INTRODUCTION

The automotive field is experiencing a fast and pervasive technological innovation that is pushing towards the realization of the new concept of the connected car [1]. Modern and forthcoming scenarios of connected cars comprise (i) vehicles capable to communicate and exchange data with other vehicles, the infrastructure, and pedestrians to share real-time traffic information and alert signals (e.g., in case of car accidents, road interruptions, or obstacles), (ii) vehicles capable to sense outside and inside the cabin to provide driving assistance and to monitor the driver's alertness and vital signs of car passengers, and (iii) vehicles that are equipped with wireless sensors and actuators capable to connect and exchange data with each other and the car's electronic control unit (ECU) through an intra-vehicle network of Internet of Things (IoT).

The technologies used to operate such services generate an electromagnetic field (EMF) at different frequencies in the radiofrequency (RF) range, from a few hundred MHz, such as in intra-vehicle IoT communication deployed with ultra-high frequency (UHF) [2], to hundreds of GHz as in radars used for in-vehicle occupant detection [3].

Many of these technologies, such as radars used for driving assistance, parking aid, and collision warning, IoT for intra-vehicle sensor network, and wireless devices used for electronic toll collection (ETC), already have a widespread use and are nowadays present as standard equipment in all new cars, whereas other technologies will see widespread use in the coming years [4]. People in a car and in the car vicinity are thus daily exposed to EMF generated by devices in the car or mounted on the car body and by devices mounted on cars in the vicinity.

The present work gives for the first time a comprehensive survey of RF EMF exposure in the specific scenario of the connected car in the RF range, from 100 MHz to 200 GHz. In our survey, we grouped the technologies according to their purpose of use, namely in (i) technologies for vehicle-to-everything (V2X) communication, (ii) technologies for car sensing, and (iii) technologies for intra-vehicle wireless communication. For each group of technologies, we describe the EMF they generate and the impact they might have on EMF exposure of car passengers and people in the car vicinity, as derived from currently available studies. Open challenges and required RF EMF characterization in the connected car are identified and discussed.

II. TECHNOLOGIES FOR VEHICLE-TO-EVERYTHING COMMUNICATIONS

First, we review the technologies for V2X communications, i.e., the communications between the vehicle and other 'entities', such as vehicles (vehicle-to-vehicle, V2V), road infrastructure (vehicle-to-infrastructure, V2I), cellular network (vehicle-to-network, V2N), and pedestrians (vehicle-to-pedestrian, V2P). V2X will be the core communication technology in fully autonomous vehicles. It is for example used to communicate safety messages, such as do-not-pass warnings, blind curve/local hazard warnings, road works warnings, vulnerable road user (e.g., pedestrian, cyclist) alerts at a blind intersection, left-turn assist, and for management of vehicle platooning. V2X also comprises ETC, a particular case of vehicular communication between a vehicle and the infrastructure for the so-called electronic toll collection services.

The main characteristics of vehicle communication technologies, including a description of their application, the relevant standards, and the characteristic of the radiated field (i.e., the operating frequency band, bandwidth, and maximum transmit power) are listed in Table 1.

If not explicitly indicated, the maximum allowed transmitted power set by the standards is the EIRP calculated as A + G + 10 log [1/DC], where A (dBm) is the measured

TABLE 1. Characteristics of technologies for V2X communications.

Application	Technology	Relevant standard	Frequency band (GHz)	Channel bandwidth (MHz)	Maximum transmitted power (dBm)
To communicate safety and non-safety messages (e.g warnings, infotraffic).	IEEE 802.11p and ITS-G5	IEEE std 802.11p [5]; ETSI EN 302 571 [6].	5.855 - 5.925	10	33 (in EU and US for non-government services) 44.8 (in US for government services)
To communicate safety and non-safety messages (e.g., warnings, infotraffic).	LTE-V2X through PC5 or Uu interface	ETSI EN 303 613 [7]; 3GPP TR 36.885 [8]; ETSI TS 136 101 [9].	5.855 - 5.925	10 or 20	23 (maximum power measured in a 1 ms frame)
To communicate safety and non-safety messages (e.g., warnings, infotraffic). For advanced driving, depending on the automation level.	5G-V2X	3GPP TR 38.886 (Rel.16) [10]; 3GPP TR 38.785 (Rel.17) [11].	ITS band: 5.855-5.925. FR1 band: 3.5 (TDD) or 2 (FDD). FR2 band: 28.	20 at ITS 5.9 GHz band; 100 or 400 at FR1 and FR2.	23
Transport and Traffic Telematics systems for ETC	DSRC	ETSI EN 300 674-2-2 [13]	5.795-5.815	0.5	14 or 21 (depending on OBU type and measured in a single side band)

If not explicitly indicated, the maximum allowed transmitted power set by the standards is the EIRP calculated as A + G + 10 log [1/DC], where A (dBm) is the measured power output of the device, DC is the duty cycle, and G is antenna assembly gain (dBi).

power output of the device, DC is the duty cycle, and G is antenna assembly gain (dBi).

V2X is operated through two main wireless access technologies, both working in the Intelligent Transport Systems (ITS) band at 5.9 GHz, namely: WiFi for mobility based on the IEEE 802.11p standard used in the US [5] and denoted as ITS-G5 in the European Cooperative Intelligent Transport Systems (C-ITS) initiative [6] and cellular technology for V2X (C-V2X) [7]–[11].

The IEEE 802.11p protocol (Table 1, first row) supports medium range (under 1 km), low latency (∼2-10 ms) and high reliability communications also in adverse weather conditions (e.g. rain, fog, snow) [12]. Communication is fully distributed among vehicles and/or road side units (RSUs), without the intervention of any infrastructure, neither for resource allocation. Communication is operated in the ITS 5.9 GHz band with a channel bandwidth of 10 MHz; the maximum power that can be transmitted by the device's antenna, as set by the standards, is 33 dBm both in EU and in the US, with 44.8 dBm also allowed in the US for government services.

C-V2X indicates an ensemble of technologies standardized by the 3rd Generation Partnership Project (3GPP) and includes V2X operated through both the Long-Term Evolution (LTE-V2X) [7]–[9] and 5G communication protocol (5G-V2X) [10], [11] and can operate via the infrastructure by using the Uu interface, i.e., the logical interface between the user equipment and the base station (e.g., to handle V2N use cases) or over the PC5 interface, enabling direct communications (also called sidelink communication) between vehicles (i.e., V2V) or between vehicles and other road users (i.e., V2P). In V2N, vehicle connectivity is obtained through the conventional cellular network to enable cloud services, such as infotainment and latency-tolerant road safety messages (e.g., information on longer-range road hazards and traffic conditions).

As far as LTE-V2X is concerned (Table 1, second row), it supports both 10 MHz and 20 MHz channels, with a maximum transmitted power of 23 dBm. LTE-V2X can operate following two resource allocation schemes, called mode 3 and mode 4 for V2X sidelink communications, i.e., for direct communication through PC5 interface. In both modes the communication between vehicles or road actors is direct, but in mode 3, the cellular infrastructure manages the resource allocation and it works just in coverage, whereas in mode 4 vehicles autonomously select, manage and configure the communication, that can, thus, works also out of coverage.

As anticipated above, C-V2X can be operated also through the 5G NR (New Radio) communication protocol (Table 1, third row). The use of 5G NR is required to enhance V2X services for future autonomous driving, which require ultra-reliable low-latency communications with high data rate and spectral efficiency. To satisfy the larger bandwidth needs of

TABLE 2. Characteristics of technologies for car sensing.

Application	Technology	Relevant standard	Frequency band (GHz)	Bandwidth (GHz)	Limit of mean transmitted power (dBm)
ADAS [a]	SRR 24 GHz NB	ETSI EN 300 440-1 [14]	24.05-24.25	0.2	20
ADAS [a]	SRR 24 GHz UWB [b]	ETSI EN 302 288-1 [15]	21.65-26.65	5	20 (measured in the 24.05-24.25 GHz band)
ADAS [c]	LRR 77 GHz	ETSI EN 301 091-1 [16]	76-77	1	23.5 (for pulsed radar); 50 (for other than pulsed radar)
ADAS [a]	SRR 79 GHz	ETSI EN 302 264-1 [17]	77-81	4	55 [d]
VOD	SRR	-	60-64 [19]-[26]; 76-81 [19]-[20]; 140 [3].	4-7 (for 60 and 76 GHz radars); 13 (for 140 GHz radar)	10-12

The mean transmitted power reported in the table is the EIRP measured during an interval of time sufficiently long compared with the lowest frequency encountered in the modulation envelope of the signal transmitted by the device under test.

[a]Typical use cases include: blind spot detection, lane-change assist, front/rear cross traffic alert. [b]UWB band is valid from Jul 2013 to 1st Jan 2018 and subsequently extended by 4 years; after 1st Jan 2022, UWB band will be phased out. [c]Typical use cases include: ACC, emergency braking. [d]Peak EIRP power in a 50 MHz band.

forthcoming advanced V2X use cases (e.g., in autonomous driving), 5G-V2X has been designed to operate not only in the ITS 5.9 GHz band (like in V2X operated through the LTE protocol) but also in the frequency range 1 (FR1, 410 MHz - 7.125 GHz) and the mmWaves frequency range 2 (FR2, 24.25-52.6 GHz).

Similarly to LTE-V2X, also 5G-V2X defines two new modes (modes 1 and mode 2) for the selection of sub-channels in 5G-V2X sidelink communications. These two modes are the counterparts to modes 3 and 4, however, LTE-V2X only supports broadcast sidelink communications while 5G-V2X supports broadcast, groupcast, and unicast sidelink communications.

Specifically, as reported in 3GPP Release 16 [10], 5G-V2X sidelink can be realized through the PC5 interface in the ITS 5.9 GHz band, in the 3.5 GHz (for time division duplex (TDD) devices) or 2 GHz (for frequency-division duplex (FDD) devices) bands for operation at FR1, and in the 28 GHz band for operation at FR2. Although 5G-V2X sidelink supports both FR1 and FR2, no specific optimization has been deployed for FR2 yet and most of the sidelink design refers to FR1. Indeed, we expect the sidelink design to be reengineered when considering the mmWave spectrum of FR2, due to its peculiarities. The channel bandwidth is 20 MHz for 5G-V2X operated at 5.9 GHz and can be as high as 100 or 400 MHz when the service is operated in FR1 and FR2, respectively. Like in LTE-V2X, the maximum transmitted power of the device is limited to 23 dBm.

Finally, ETC (Table 1, last row) is a short-range radiocommunication technology between a roadside infrastructure and a vehicle or a mobile platform [13]. In addition to electronic toll collection *per se*, applications of ETC technology include parking payment, gas (fuel) payment, in-vehicle signing, traffic information, management of public transportation and commercial vehicles, fleet management, weather information, electronic commerce, probe data collection, highway-rail intersection warning, tractor-to-trailer data transfer, other content services, border crossing, and electronic clearance of freight. ETC is operated in the 5.795-5.815 GHz band, with a 0.5 MHz channel bandwidth; the maximum transmitted power of an ETC on-board unit (OBU) ranges from 14 to 21 dBm.

III. TECHNOLOGIES FOR CAR SENSING

Second, we review technologies used by automotive radars mounted on the car body or in the car cabin. Radars mounted on the car body are used in advanced driver-assistance system (ADAS) applications to detect the presence of objects in the vicinity of the vehicle. Recently, radars are being used also inside the vehicle for vehicle occupant detection (VOD) applications, which aim to detect the presence of people inside the car and warn the driver of passengers left in the rear seats when the driver exits the car.

The main characteristics of car sensing technologies, including a description of their application, the relevant standards, and the characteristic of the radiated field (i.e., the operating frequency band, bandwidth, and maximum transmit power) are reported in Table 2.

In ADAS, radars are mounted on the car body to sense the surroundings of the car and acquire information, such as the distance, velocity, direction, and angular position of objects that are in the radars' range. This information is processed by the central processing unit or field-programmable gate array of the car to provide vehicle control corrections, collision

warnings, and to prevent vehicle from accelerating into the front of vehicles or pedestrians ahead. ADAS is the core technology of the forthcoming fully autonomous vehicle. Depending on the specific application, ADAS is deployed through radars with a range from 1 to 250 m. ADAS radars are operated in the 24, 77, and 79 GHz band and can use pulse Doppler or frequency-modulated continuous wave (FMCW) technology [14]–[17]. The limit for the transmit power is typically around 20 dBm; however, depending on the type of technology, it can be as high as 50 dBm.

Recently, automotive radars are being used also in VOD applications (see, e.g., [3], [18]–[26]) to detect how many passengers are in the car and which seats are occupied by passengers. Most VOD applications are able to recognize also the type of passenger in the car, distinguishing adults, little children, or even animals, and can record passenger breathing movements, generating warnings when these movements are different from what is expected from a healthy subject.

Although radars for VOD applications are already available on the market (see e.g., [19]–[26] in last row of Table 2), their use is not yet formally standardized. This lack of standards / regulations specific to the use of radars inside a vehicle means that there is not yet a consensus among the manufacturers on the band at which the service is operated nor on the maximum transmitted power. From the review we made of the systems on the market, it appears that VOD radars are typically operated in the 60 GHz [19]–[26], 77 GHz [19], [20] and 140 GHz band [3]; usually, they are operated at significantly lower transmission power than in ADAS application, typically at 12 dBm.

IV. TECHNOLOGIES FOR WIRELESS INTRA-VEHICLE COMMUNICATION

Finally, in this group we review the technologies for wireless connectivity within the car and their typical applications, as listed in Table 3.

Current cars are typically equipped with around 60-100 different on-board sensors to monitor the health of vehicle parts and to measure and control the vehicle's asset and performance. The number of on-board sensors is expected to grow in the forthcoming years due to the increasing demand of more efficient and sustainable cars, supporting a higher degree of automation. On-board sensors can be connected directly to the car ECU through cables or, to reduce the wiring, through a CAN (Controller Area Network) communication bus shared among all ''active'' sensors. In any case, wire-only or CAN bus connection alone might be no more sustainable in modern and forthcoming cars, especially for those vehicles with a high degree of automation, as the cables needed to connect such a great number of sensors would increase the car weight and costs and diminish the fuel efficiency.

Wireless technology is frequently used in modern cars as a viable solution to replace (whenever possible) the sensors' cables, as for example to replace with a wireless link the cables between the car windows, the mirrors, and the ECUs and to allow monitoring moving and difficult to access parts that can not be reached through a wired link, such as the tires.

Typical applications of intra-vehicle wireless connectivity are vehicle diagnostics, smart car access, in-vehicle control and personalization, infotainment, and in-cabin multimedia transmission [27]–[35]. As to vehicle diagnostics, wireless technology is used for example to: measure the temperature of the brake discs through wireless sensors mounted directly on the wheels of the car; measure in tire pressure monitoring system (TPMS) applications the tire's air pressure and temperature through a wireless sensor mounted on the tire valve; measure the level and flow of the fuel, the strain and vibration of the chassis, the torque of drive train, the engine's valves displacement, the vehicle orientation and dynamics, the acceleration and displacement of the suspension system; in case of an accident, to measure the severity and the location of the impact on the vehicle.

In addition to vehicle diagnostics, wireless intra-vehicle connectivity is used for in-vehicle control and personalization such as in passive entry passive start (PEPS) modules that enable to unlocking the car and starting the engine with a smartphone, key fob or a smart card holding a digital key and for in-vehicle control services that allow the car to automatically recognize the driver's smartphone and activate interior and/or exterior lighting, adjust seating, ventilation and air conditioning settings.

Finally, a common use of intra-vehicle wireless connectivity is for multimedia transmission within the vehicle cabin (e.g., for displaying multimedia contents to the screens of the rear passengers) and for pairing the smartphone to the car's infotainment central unit to access to navigation, music and phone apps through the car dashboard while driving.

The main characteristics of intra-car wireless communication technologies, including a description of their application, the relevant standards, and the characteristic of the radiated field (i.e., the operating frequency band, bandwidth, and maximum transmitted power) are listed in Table 3. As reported in Table 3, intra-car wireless communication is deployed on current vehicles through Bluetooth low energy (BLE), UHF short range communication, ultra-wide band (UWB) communication, and near-field communication (NFC).

BLE is a short range communication developed by the Bluetooth Special Interest Group and is characterized by ultra-low power consumption and transmission efficiency [36]–[40]. BLE is operated in the 2.4 GHz industrial, scientific and medical (ISM) band and supports up to 100 mW (+20 dBm) transmitted power.

UHF short range communication [41]–[45] is used in automotive connectivity for enabling TPMS and remote keyless entry (RKE) services; it is operated in the 315, 434, and 868 MHz bands and supports up to 10 or 25 mW transmitted power, depending on Regional regulations and operating band.

UWB is a short range communication that uses a relatively large bandwidth of 500 MHz or more and/or a bandwidth that is at least 20% the carrier frequency [46]–[48]. It is operated

TABLE 3. Characteristics of technologies for intra-vehicle wireless communication.

Application	Technology	Relevant standard	Frequency band (MHz)	Channel bandwidth	Radiated emission limits for transmitter
Smartphone pairing to the infotainment central unit of the car; multimedia in-cabin transmission; smart car access/start (incl. RKE, PaaK, PEPS); vehicle diagnostics (including TPMS); in-vehicle control settings.	BLE	IEEE 802.15.1 [36]; ETSI EN 300 328 [37]; EN 300 440 [38]; EN 301 489-17 [39]; Bluetooth Core Specification [40].	2400-2483.5	2 MHz	20 dBm
TPMS and RKE.	UHF short range	ETSI TR 102 649-2 [41]; EN 300 220-1 [42] and EN 300 220-2 [43]; ERC Recommendation 70-03 [44]; 47 CFR-Part 15 [45].	Europe: 434, 868. US: 315, 434.	Europe: ~200 kHz. [a] US: 785.5 kHz at 315 MHz; 1.085 MHz at 434 MHz.	Europe: 10 mW ERP at 434 MHz; 25 mW ERP at 868 MHz. US: 200 µV/m at a distance of 3 m.
Smart car access (RKE); gesture recognition (e.g., to open car tailgate); recognition of child seats location and deactivation of corresponding airbag; automated trailer attach (clever trailer coupling).	UWB communication	47 CFR-Part 15-Subpart F [46]; ETSI EN 302 065-3 [47]; IEEE 802.15.4z [48].	Europe: 3100-4800 and 6000-9000; US: 3100-10600.	≥500 MHz or ≥20% the carrier frequency.	-41.3 dBm/MHz
Smart car access/start (incl. PEPS, key less entry); Bluetooth/WiFi pairing with the car infotainment central unit.	NFC	ISO/IEC 18000-3 [49]; ETSI EN 300 330 [50]; ERC Recommendation 70-03 [44].	13.56	For narrowband NFC: 200 kHz. For wideband NFC: 14 MHz.	For narrowband NFC: 60 dBµA/m. [b] For wideband NFC: 42 dBµA/m. [b]

ERP (effective radiated power): it is the power radiated in the direction of the maximum radiated power. [a]Specifically indicated for automotive applications [41]. [b]H-field strength limit at a distance of 10 m.

in the unlicensed 3.1-10.6 GHz band and supports a mean power spectral density of −41.3 dBm/MHz.

Finally, NFC is a short range, [49], [50]; by using magnetic induction, it enables the exchange of data and transfer of power between devices by bringing them into close proximity to a distance of a few centimeters. NFC is operated at 13.56 MHz and supports a magnetic field (H-field) limit of 42 dBμA/m or 60 dBμA/m, depending on the bandwidth of the device.

V. EMF EXPOSURE ASSESSMENT IN THE CONNECTED VEHICLE

In the current Section V, we describe the main evidences from currently available literature on the assessment of the exposure field and the dose absorbed by passengers of cars equipped with the technologies previously described. In March 2022, we performed a literature search without time constraints in the Scopus and Web of Science (WoS) databases. We queried Scopus and WoS using the terms ''electromagnetic field'', radar/pulsed fields/millimeter wave/UWB/ultra-wideband/RF exposure/dosimetry/SAR, and vehicle/car/automotive in the title, keywords, and abstracts of articles, conference papers, and book chapters. The query resulted in 526 unique papers (combining both databases). From these originally retrieved papers, we discarded: papers that analyzed technologies and frequencies different from those used in the connected car; papers that did not report the basic details on the analyzed exposure setup (e.g., antenna characteristics, number and position of antennas) and quantitative data either on the exposure field emitted by the device under test or on the dose absorbed by the people in the vicinity of the device; and papers from the same team of authors reporting duplicate results. As a result, we retained in the present survey 32 papers that will be analyzed in the following Sections.

A. GENERAL ELECTROMAGNETIC CHARACTERISTICS OF THE CAR AS EXPOSURE SCENARIO

Due to its partially closed structure, the car is a peculiar exposure scenario, which can generate standing waves and a loss of the power transmitted in the cabin from a source external to the vehicle (e.g., an antenna mounted on the car roof).

As to standing waves, Hirata and Ida [51] found that the electric field (E-field) induced inside the car by an external plane wave at 10 MHz-1 GHz was enhanced at ∼120 MHz,

due to the standing waves generated inside the vehicle cabin. Standing waves were suppressed in the 100-200 MHz range when a human body was present inside the vehicle, due to the power absorbed by the car occupant [51]. Also, in the frequency region of standing wave suppression (i.e., at 100-200 MHz), the dose of EMF absorbed by the car occupant at the whole-body level was lower inside the car than in free space [52]. Vice versa, at frequencies outside the 100-200 MHz range, the presence of a car occupant had only a marginal effect on the suppression of the standing waves [51]. The frequency region at which standing waves were suppressed depends on the dimension of the vehicle cabin and the number and size of car windows. The presence of passengers in the car generated a similar suppression effect of also the exposure field: as observed in [53], the average in-vehicle E-field was lower in the presence of passengers than in an empty car.

The car body structure (i.e., the full-vehicle) also causes a loss in the penetration inside the car of fields generated by antennas mounted on the roof of the car or mounted on the road infrastructure. The amount of penetration loss (defined as the ratio of the received power immediately outside the vehicle to the received power inside the vehicle) depends on the size of the car and the number and size of the car windows. As observed in [54], RF penetration loss due to the car body could be as high as 3.2-23.8 dB at 600-2400 MHz. As a consequence, it is expected that EMF exposure generated by sources external to the vehicle would be lower inside the vehicle cabin than outside.

B. THE LIMITS FOR EXPOSURE IN THE RF RANGE 100 KHZ - 300 GHZ

Absorption of RF EMFs can generate a temperature rise in the body. The exposure limits recommended by the International Commission on Non-Ionizing Radiation Protection (ICNIRP) [55] and IEEE [56] were set to keep the local and core body temperature rise to a safe level. Namely, compliance with these latter limits would provide a protection against potential adverse health effects that are observed when the core body temperature increases over 1 °C and local body temperature increases more than 5 °C for Type-1 tissues (all tissues in the upper arm, forearm, hand, thigh, leg, foot, pinna and the cornea, anterior chamber and iris of the eye, epidermal, dermal, fat, muscle, and bone tissue) and 2 °C for Type-2 tissues (all tissues in the head, eye, abdomen, back, thorax, and pelvis, excluding those defined as Type-1 tissue) [55].

As to core body temperature rise, the *basic restrictions* for exposure in the RF range 100 kHz - 300 GHz [55], [56] are set in terms of the specific energy absorption rate (SAR) at the whole body, that is the power absorbed per unit mass of the entire body. For the general public, the whole body SAR exposure limit is equal to 0.08 W/kg, averaged over 30 minutes of exposure [55], [56]. As to local body temperature rise, the basic restrictions for exposure fields within the 100 kHz - 6 GHz range are set in terms of the local SAR averaged over 10 g of mass, with a limit of 2 W/kg and 4 W/kg for local exposure at the head/torso and the limbs, averaged over 6 minutes [55], [56]. For frequencies within the >6 GHz – 300 GHz range, as the RF energy is deposited mainly at superficial tissues and not in deeper tissues as for lower frequencies, the basic restrictions are set in terms of the local absorbed power density (S_{ab}), that is the density of the power absorbed over a square 4-cm^2 surface area of the body; the limit is set to 20 W/m^2, averaged over 6 minutes [55], [56].

In case in which it is not feasible to measure the power absorbed in the body, it is possible to assess compliance with the so-called *reference levels* that are based on exposure quantities that shall be measured outside the body, that is the incident E-field and H-field strength and the incident power density. For exposure in the far-field zone at frequencies ≤2 GHz, compliance shall be assessed with either the E-field or H-field or the incident power density reference levels; these latter reference levels depend on the frequency of the emitting source [55], [56]. For frequencies >2 GHz, like in automotive radars and V2X communication, compliance shall be assessed with the reference level based on the incident power density only, which is equal to 10 W/m^2 averaged over 30 minutes, at any frequency >2 GHz [55], [56].

C. METHODS FOR RF EXPOSURE ASSESSMENT

Table 4 and Table 5 list an overview of EMF exposure assessment in the car at frequencies used in V2X communication, intra-car communication, and generic wireless communication services used in the car (Table 4) and in the 24-100 GHz band of automotive radars (Table 5).

For each study listed in Table 4 and Table 5, we report all the relevant details, namely the frequency, the power, and the directivity gain or type of the investigated RF antenna, the method used to assess the exposure inside the car, the use-case (i.e., exposure scenario) addressed, the estimated / measured exposure quantity, and the main outcomes. For the sake of clarity, we preferred to put all the analytical details of the studies in Table 4 and Table 5, while we resumed in the following paragraphs only the main outcomes by grouping the studies in clusters with similar research aims and setups.

As described in Table 4 and Table 5, in-cabin field exposure assessment was typically performed through experimental measurements and numerical simulations. In experimental studies (see [61], [63]–[68] in Table 4 and [79], [80] in Table 5), the aim was to measure inside the cabin of a real vehicle the field exposure generated by one or more RF device placed either outside (e.g., on the car roof, on the road infrastructure such as base stations, and on other cars in the nearby such as ADAS radars mounted on approaching cars) or inside the car (e.g., at the front dashboard). Measurements were done in the empty car (i.e., with no car occupants inside) at typically the driver and passengers' seats to assess compliance with exposure limits in the most critical positions, that is the positions occupied by car passengers. All experimental

studies ([61], [64]–[68], [79], [80]) but [63], measured the E-field: as such, for these former studies, the compliance with exposure limits can be assessed by comparing the measured E-field against the reference E-field level in [55] and [56]. Instead, the latter study [63] measured the SAR inside an anatomically-realistic adult human phantom that consisted of a fiberglass shell filled with a material of the same dielectric properties of the human muscle tissue. The phantom was seated inside a real car; SAR was measured by placing the measuring probe in the phantom's head. For this latter study, the compliance with exposure limits can be assessed by comparing the measured SAR against the basic SAR restrictions in [55] and [56].

In numerical simulation studies (see [57]–[60], [62], [69]–[78] in Table 4 and [57], [81]–[84] in Table 5) the aim was to estimate the exposure field using numerical methods capable to calculate electromagnetic quantities, such as the E-field and H-field, as generated by a simulated source in a simulated exposure scenario.

The numerical simulation approach can be purely analytical or can use computational electromagnetic methods. Any analytical approach relies on a strong simplification of the exposure scenario and does not allow taking into account the potential effects on the exposure field of the real 3D geometrical shape neither of the car nor the emitting antenna. For example, in [57] an analytical approach – the power balance method [86] – is applied to estimate the average E-field strength inside a vehicle cabin in the 0.9-5.8 GHz frequency range. The application of the power balance method relies on the assumption that at frequencies above ∼1 GHz, the vehicle cabin can be approximated as an electrically large cavity where the average internal E-field strength is a function of basically only the windows' size and glazing materials [57]. The output of an analytical approach is typically the E-field strength and the power density; compliance with exposure limits shall thus be assessed using reference levels in [55] and [56]. Being based on strong approximations, the analytic approach is useful to gain a first insight on the exposure field when it is not possible to implement more computational demanding methods capable to model and take into account the 3D geometry of the exposure scenario (i.e., the car, the emitting antennas, and the car's occupant(s)).

In addition to the analytical approach described above, numerical simulation of the exposure field can be done also using computational electromagnetic approaches capable to solve Maxwell's equations directly, as the Finite-Difference Time-Domain (FDTD) method [87]. Examples of application of computational electromagnetics for field exposure assessment in the car are in [58]–[60], [62], [69]–[78] in Table 4 and [81]–[84] in Table 5. In computational electromagnetics, the exposure scenario is modelled using 3D geometries; the scenario is then discretized in terms of grids and Maxwell's equations are solved at each point in the grid. The discretization level in a FTDT grid does not depend on geometrical dimensions, but rather on the electrical dimensions of the objects as it is normalized to the minimum wavelength among all materials considered in the simulation. The scenario typically includes the 3D geometric model of the emitting antenna(s) (that could be as schematic as a simple monopole/dipole antenna or more complex as a 3D model of the entire emitting device, case included), the 3D geometric model of the car (simplified or a realistic CAD model) and the 3D human phantom (simplified as a spheroid or detailed and anatomically realistic, including all organs and body tissues). Computational electromagnetic approaches allow the computation of electromagnetic quantities both in the space around the human phantom and, most important, inside the phantom (and in every tissue/organ), being thus a consolidated and robust methodology to assess the SAR and the S_{ab} in the body and its tissues. The drawback of computational electromagnetic approaches is that they are computationally demanding, especially when the simulated exposure scenario has a dimension much greater than the minimum wavelength in the considered computational volume, like in automotive scenarios.

D. IN-CABIN FIELD EXPOSURE ASSESSMENT TO FREQUENCIES USED IN V2X, INTRA-CAR AND GENERIC IN-CAR WIRELESS COMMUNICATION

Table 4 gives an overview of EMF assessment in cars in the 100 MHz – 10 GHz range that covers V2X communication, intra-car communication, and generic wireless communication services used in the car, such as mobile communication, WiFi, and Bluetooth. We grouped the studies in Table 4 in three clusters based on the scenario they addressed, that is: specific V2X exposure scenarios (Section D.1) and generic in-car connectivity exposure scenarios generated either by antennas external to the car (Section D.2) or antennas placed inside the car (Section D.3).

1) IN-VEHICLE EXPOSURE FROM SPECIFIC V2X COMMUNICATION

To the best of the authors' knowledge, there are only a very few studies ([57], [58], [59]) on EMF exposure in specific V2X scenarios, whereas most of the past studies focused on in-vehicle exposure from generic wireless communication used in cars, such as mobile communication (e.g., Global System for Mobile Communications-GSM, Universal Mobile Telecommunications Service-UMTS, and LTE), Bluetooth and WiFi.

As to exposure assessment in V2X scenarios, a first attempt was done by Ruddle [57] (Table 4) that used a simplified analytical approach for evaluating the field coupled inside a car from an external ETC device (a toll beacon) at 5.8 GHz. The ETC device was simulated at the maximum allowable Effective Isotropic Radiated Power (EIRP), at 5 m from the car. Results evidenced that the power density coupled inside the vehicle was 0.005 W/m^2, that is well below the safety reference level of exposure of 10 W/m^2 for the general population [55], [56].

A more realistic and complex exposure scenario was addressed for the first time by Tognola *et al.* [58], [59]

TABLE 4. Studies on EMF exposure assessment inside the car – frequencies from 100 MHz to 10 GHz.

Study name	Frequency, power and directivity gain or type of analyzed EMF source	Study type and setup	EMF source position re: vehicle cabin	Quantity measured/estimated & main study outcomes
		Specific V2X exposure scenario		
Ruddle [57]	5.8 GHz at 33 dBm (2 W) EIRP, plane wave.	Analytical simplified model of in-vehicle E-field strength.	External: DSRC device (toll beacon) at 5 m from the car.	Power density coupled inside the vehicle cabin: 0.005 W/m^2.
Tognola *et al*. [58], [59]	ITS 5.9 GHz at 33 dBm EIRP, quarter-wave monopole.	Numerical simulation using a realistic 3D model of a car and an adult human phantom as a car passenger (at the driver position).	External: four V2V antennas mounted on the roof of the car.	Whole body SAR and peak SAR_{10g}: the maximum value of SAR was obtained with four antennas and was equal to 0.008 W/kg for the whole body, 1.58 W/kg at the head/torso, and 0.76 W/kg at the limbs.
		Generic wireless communication exposure scenario: antennas outside the vehicle cabin		
Baramili *et al*. [60]	LTE: (690-960 MHz), (1710-2170 MHz), (2400-2700 MHz). 5G: (600-960 MHz), (3300-5000 MHz), conformal multi-band antenna [a]	Numerical simulation using a 3D model of a car with a realistic human phantom at the driver position.	External: one antenna integrated in the glass of either the front or rear window.	E-field inside the vehicle cabin at the driver position: for all bands and the two antenna positions, the maximum was below 24 V/m.
Tarusawa *et al.* [61]	900 MHz at 1 W input power. Three types: space diversity vertical antenna (trunk-lid antenna); vertical dipole (rear-window antenna); 5/8 wavelength whip antenna (roof antenna).	Experimental measurement of E-field inside the cabin of a real car.	External: one antenna mounted either on the car roof or the trunk lid or the rear window.	E-field inside the vehicle cabin: the maximum was 8 V/m, 30 V/m, and 32 V/m as generated by the trunk-lid, the rear window, and the roof antenna respectively.
Ruddle *et al.* [62]	400 and 900 MHz at 1 W, quarter-wave monopole.	Numerical simulation using a 3D model of a car and 4 human phantoms as car passengers.	External: one antenna mounted outside on the car's roof.	Whole-body and local SAR: the highest SAR was obtained for the whole-body at 400 MHz and was below 0.6% of the basic restrictions.
McCoy *et al.* [63]	VHF (146 MHz) at 100 W; UHF (460 MHz) at 102 W. Quarter-wave monopole.	Experimental measurement of SAR in a adult human phantom seated inside the car.	External: antenna mounted on the trunk of the car.	Peak SAR_{1g}: the highest value was around 2.3 mW/kg for both frequencies and was observed in the head region.
		Generic wireless communication exposure scenario: antennas inside the vehicle cabin		
Anzaldi *et al.* [64]	GSM 1800 MHz, quarter-wave monopole [a]	Experimental part: measurement of E-field inside the vehicle cabin. Numerical simulation: field calculation inside the vehicle cabin using a 3D model of the car and the antenna.	Internal: one antenna mounted at the center of the cabin's roof.	E-field inside the cabin: the maximum was 7 V/m (measured experimentally) and 7.4 V/m (estimated from numerical simulations).
Rodrigues *et al*. [65]	2.047 GHz at 500 mW input power, quarter-wave monopole.	Experimental measurement of E-field inside two real cars of different size (compact and sedan models).	Internal: four antennas mounted at the front and rear passenger seats, at an height of an hand-held used phone.	E-field inside the vehicle cabin: the maximum value estimated at the driver, front passenger and rear seats was achieved when all antennas were switched on and was within 18 V/m.

TABLE 4. ***(Continued.)*** **Studies on EMF exposure assessment inside the car – frequencies from 100 MHz to 10 GHz.**

Buckus *et al*. [66]	GSM 900 and 1800 MHz band at 0.25-2 W maximum output power level, real GSM phone antenna.	Experimental measurement of E-field in a real car driving in the 200 m beam (urban area) and 1000 m beam (rural area) of the BS.	Internal: various GSM phones with different power levels, used inside the car during an outgoing call.	E-field inside the vehicle cabin: at 20 cm from the phone, the maximum value was 7 V/m in urban area, obtained with a GSM 1800 (1 W) and 10 V/m in rural area, obtained with a GSM 900 (2 W) phone.
Psenakova *et al*. [67]	Bluetooth 2400 MHz; GSM 800 MHz; UMTS 2100 MHz. Real GSM/UMTS phone antenna[b]	Experimental measurement of E-field during a phone call inside a real car equipped with built-in Bluetooth connectivity.	Internal: a GSM/UMTS phone placed on the dashboard compartment of a car equipped with a built-in Bluetooth antenna.	E-field inside the vehicle cabin, measured at the chest level of the driver: the maximum was around 48.48 mV/m at 800 MHz,72.54 mV/m at 2100 MHz, and 218.1 mV/m at 2400 MHz.[c]
Aguirre *et al*. [68]	ZigBee (2.4 GHz) at 63 mW, omnidirectional antenna, 1.5 dBi gain. GSM (900 and 1800 MHz) and UMTS (2100 MHz), real phone antenna.[d]	Experimental measurements of E-field inside the cabin of a real vehicle in an urban area.	Internal: a ZigBee antenna and a multi-band GSM/UMTS placed on the front dashboard.	E-field inside the car: the maximum value generated by the ZigBee antenna was 2 V/m; for GSM and UMTS, the maximum was below 1.5 V/m.
Ruddle [57]	0.9/1.8/2.1/2.4 GHz at 1 W radiated power, plane wave.	Analytical estimation through power balance methods of in-vehicle E-field strength.	Internal: simulated in-vehicle transmitters equivalent to mobile phones (at 0.9/1.8/2.1 GHz) and personal devices (2.4 GHz WiFi and Bluetooth).	E-field inside the vehicle cabin: the average value was below 25 V/m RMS for 1 W of radiated power, at all frequencies. When devices were operated at their maximum EIRP, the highest value of the E-field was 31.8 V/m and was generated by the 0.9 GHz device at 2 W EIRP.
Low and Ruddle [69]	900, 1800, 2400 MHz at 1 W radiated power, quarter-wave monopole.	Numerical simulation with a realistic 3D model of a car to estimate E-field inside the car cabin.	Internal: one antenna placed inside the cabin either at the top of the windscreen or on a storage box located between the two front seats.	E-field inside the car: the highest average value (19.03 V/m) was at 900 MHz. At 1800 and 2400 MHz the average E-field was slightly lower.
Toropainen [70]	AMPS (800 MHz), GSM (900, 1800 MHz), and CDMA (2000 MHz), generic omnidirectional antenna.[e]	Numerical simulation to estimate the equivalent power density and whole-body SAR inside a resonant metal cavity with dimensions of a real car.	Internal: mobile phones placed inside the cavity.	Basic restriction limits are exceeded only when using 30-160 mobile phones operated at the same time at their maximum power in the car, i.e., with a number of devices much higher than the number of possible users in the car.
Lee *et al*. [71]	1-3 GHz half-wave dipole; the antenna input power was adjusted to generate an equivalent E-field level of 1 V/m inside the vehicle cabin (no passengers inside).	Numerical simulation using a 3D model of a car and a homogeneous spheroid mimicking a person at the driver position.	Internal: one antenna with horizontal or vertical polarization, mounted at different places inside the cabin.	Whole-body SAR: the highest value (14 μW/kg) was obtained at 1 GHz with an horizontally polarized antenna mounted at the middle of the car dashboard.
Anzaldi *et al*. [72]	835 MHz at 0.58 W radiated power, half-wave dipole.	Numerical simulation using a 3D model of the car, a human phantom seated inside the car, and a phone.	Internal: phone in hands-free use (placed to the right of the steering wheel) and hand-held use (phone held by the	SAR evaluated over three planes: at the heart, thighs, and eye level.[f] In hands-free use, the maximum SAR of 56 mW/kg was at heart plane level, in the right arm; in hand-held use, the maximum SAR of 2 W/kg was at the eye plane level, at

TABLE 4. *(Continued.)* **Studies on EMF exposure assessment inside the car – frequencies from 100 MHz to 10 GHz.**

			front passenger, close to the right side of the head)	the right side and 15 mm toward the interior of the head.
Chan *et al*. [73]	900 MHz at 2 W radiated power, quarter-wave monopole.	Numerical simulation with a simplified 3D model of a car and simplified human phantoms as car passengers (4 in total).	Internal: a simplified 3D model of the emitting device (a phone) is placed at ear level near the head of the user (single user).	The highest SAR (0.472 W/kg) was observed with 4 people (1 user + 3 passengers) in the car.
Leung *et al*. [74]; Diao *et al*. [75]	900 MHz at 2 W; 1800 MHz at 1 W; 2400 MHz at 0.1 W. Quarter-wave monopole.	Numerical simulation with a simplified 3D model of a car and simplified human phantoms as car passengers (5 in total).	Internal: a simplified 3D model of the emitting device (a phone) is placed at ear level near the head of the user(s). One- and two-user conditions are considered.	Single-user condition: the highest SAR_{10g} was 3.02 W/kg at 900 MHz, 1.88 W/kg at 1800 MHz, 0.19 W/kg at 2400 MHz. Two-user condition: the highest SAR_{10g} (3.77 W/kg) was observed using two phones operated at 900 MHz. Other combinations of phone/frequencies resulted in lower SAR values.
Ruddle *et al.* [62]	400, 900, 1800, and 2400 MHz at 1 W, quarter-wave monopole.	Numerical simulation using a 3D model of a car and 4 human phantoms as car passengers.	Internal: one antenna mounted inside the vehicle cabin.	Whole-body and local SAR: the highest SAR was at 400 and 900 MHz (equal to 9.9% and 8.6% of basic restrictions, respectively); SAR at 1800 and 2400 MHz was lower (4.6 % and 3.6% of basic restrictions, respectively). The head and trunk were the regions with the highest SAR at 900, 1800, and 2400 MHz; at 400 MHz, the highest SAR was at the whole-body level.
Harris *et al*. [76]	UMTS (2.1 GHz) at 125-250 mW radiated power, inverted F-type antenna; WiMax (2.5 GHz) at 200 mW radiated power, generic monopole; Bluetooth (2.45 GHz) at 2 mW, generic monopole.	Numerical simulation using a 3D model of a car and human phantoms of adult and child passengers in the car.	Internal: the emitting devices were placed inside the vehicle cabin at the driver and passenger seats. Single-user (i.e., only one device operated at a time) and two-user (two devices operated at the same time) scenarios were evaluated.	Whole-body SAR: the highest value was obtained in the two-user scenarios with two UMTS devices and was equal 2.13 mW/kg. Local SAR_{10g}: the highest value in the head/trunk was obtained with UMTS and was equal to 25.3 mW/kg; in the limbs, the highest value was obtained with the WiMax device and was equal to 392.6 mW/kg. The contribution of the Bluetooth device to the SAR is not significant. In all conditions, the highest SAR was observed in the configuration with 1 adult + 3 children as car passengers.
Jeladze *et al*. [77]	450, 900, and 1800 MHz bands at 1 W. Type of antenna: not specified.	Numerical simulation using a 3D model of a car and a human phantom at the driver position.	Internal: a mobile phone antenna at 2.5 cm from the phantom head.	Point SAR: the maximum was 96 W/kg at 450 MHz, 296 W/kg at 900 MHz, and 127 W/kg at 1800 MHz.
Aminzadeh *et al*. [78]	Bluetooth 2400-2450 MHz at 2.5 mW, planar inverted F-antenna.	Numerical simulation: 3D model of a car with a human phantom inside, wearing a mobile headset. For the human phantom, only the head was modelled.	Internal: one headset worn at the left ear of the passenger.	SAR_{1g} and SAR_{10g}: the maximum was observed at the ear level and was equal to 0.1153 W/kg for SAR_{1g} and 0.0486 W/kg for SAR_{10g}.

[a]The paper does not report the radiated power of the analyzed antenna. [b]The devices under analysis are the built-in Bluetooth module that allows to pair the smartphone with the car dashboard and a smartphone operating in the GSM/UMTS band. No indications are given on the actual power radiated by these devices. [c]All values reported in this Table were measured during the phone call, with also the car's Bluetooth activated. [d]GSM and UMTS transmitters were operated in real conditions, i.e., with transmitted power dynamically set by the power control unit of the device. [e]The simulated devices (mobile phones) are operated at their maximum power level, that is at 600 mW for AMPS, 250 mW for GSM-900, 125 mW for GSM-1800, and 200 mW for CDMA. [f]SAR computed in a cell of 27 mm^3 of volume, corresponding to about 27 mg of mass. It is not a SAR averaged over 10 g.

(Table 4) who assessed RF exposure in a realistic anatomical human phantom seated at the driver position inside a 3D model of a real city car equipped with V2V external antennas mounted on the roof. The dose absorbed by the driver at the typical V2V ITS 5.9 GHz band was quantified as the SAR. As observed in [58], [59], the dose was mainly absorbed at the most superficial tissues of the body - the skin - and in the head.

In the worst-case scenario (that consisted of four antennas operated at the same time and at the maximum EIRP) the dose absorbed by the whole body (0.008 W/kg), at the head/torso (1.58 W/kg), and the limbs (0.76 W/kg) was well below the basic restriction limit for EMF exposure of the general population at 100 kHz-300 GHz, which is equal to 0.08 W/kg for the whole body, 2 W/kg in 10 g tissue for the head/torso, and 4 W/kg in 10 g tissue for the limbs [55], [56].

2) IN-VEHICLE EXPOSURE FROM GENERIC IN-CAR WIRELESS COMMUNICATION – EXTERNAL ANTENNAS

The remaining studies listed in Table 4 investigated in-vehicle field exposure generated at the frequencies used in generic wireless communications by external (described in this current Section D.2) and internal antennas (Section D.3).

As to external antennas, studies [60]–[63] in Table 4 addressed antennas mounted on the car body in the Very High Frequency-VHF (146 MHz), UHF (460 MHz), GSM (900 and 1800 MHz), 5G NR (600 and 3500 MHz), and WiFi (2400 MHz) bands. In all studies, in-cabin exposure field was found to be below the reference level of exposure of 27.7 V/m at 146 MHz, 29.5 V/m at 460 MHz, 41.25 V/m at 900 MHz, 58.3 V/m at 1800 MHz, 67.4 V/m at 2400 MHz, and 81.3 V/m at 3500 MHz as set in [55], [56]. Similarly, the dose absorbed by the passengers in the car was below the basic restrictions for the general public at all bands mentioned above. As a general remark, the highest exposure was observed at the whole body and in the head region [62], [63].

3) IN-VEHICLE EXPOSURE FROM GENERIC WIRELESS IN-CAR COMMUNICATION – INTERNAL ANTENNAS

Studies [57], [64]–[78] in Table 4 addressed EMF exposure from antennas and devices operated inside the vehicle, such as mobile phones (GSM 900 and 1800 MHz and UMTS 2100 MHz) and Bluetooth, WiFi, and ZigBee devices.

Field exposure inside the vehicle cabin measured experimentally [64]–[68] or assessed with numerical simulations [57], [62], [69], [71]–[78] was again below the reference level of exposure, at all tested frequencies. The dose absorbed by the passenger closer to the emitting device(s) slightly increased with the number of car occupants (see e.g., [73]) and the number of devices simultaneously used in the car (see e.g., [74], [75]). In any case, the dose of exposure was always below the basic restriction limits [55], [56].

Although in all above studies the exposure field was found to be in anyway below the reference levels and the dose absorbed by car passengers was below the basic restrictions limits, results listed in Table 4 need some comments:

1) Some measured and reported scenarios are not realistic, practical or have ever been really implemented but correspond to the so-called ''worst-case scenario'', that is a scenario where the source is intentionally mounted on the car body or in the car cabin in places that would be most critical for the level of RF exposure but are not used in real settings. This was done to assess what would be the maximum exposure in the worst case. Examples of such scenarios are in [61] and [64], where the studies' outcome evidenced unusual electric field values that deviate from everyday exposure levels.
2) In some experimental studies (e.g., [61], [64]–[66]) values of field exposure are quite large because of the intrinsic limitations of performing measurements close to so large metallic structure as the car body. In general, in experimental studies measurement uncertainty plays an important role and should be taken into consideration in the interpretation of the results.

E. IN-CABIN FIELD EXPOSURE ASSESSMENT TO FREQUECIES USED IN AUTOMOTIVE RADAR APPLICATIONS

Table 5 summarizes the outcomes from studies on field exposure at radar frequencies, i.e., 24-100 GHz.

As a general remark, we did not find any study addressing realistic scenarios of automotive applications of radars. The best approximation of a realistic automotive radar scenario was in [79] and [80]. Study [79] assessed the exposure from automotive radars by applying a horn antenna to measure the increase of the superficial temperature of the human skin and porcine eye. The horn antenna was fed with a continuous wave at 1-10 mW/cm^2 power density at 77 GHz. The measured temperature rise was well below the safe limit of 2-5 °C even at an incident power density of 10 mW/cm^2 (=100 W/m^2), which is ten times greater than the reference exposure limit [55], [56]. In [80], a 79 GHz automotive radar is analyzed to measure the power density emitted at 3-30 mm distance in the worst case scenario of 100% duty cycle and maximum output power. The study evidenced that the power density averaged over 1 cm^2 was below the limits for exposure [55], [56].

Another quite realistic scenario was addressed in [57] that analytically estimated the effect of the car body on the field coupled inside the vehicle cabin. In [57], it is observed that the power density coupled inside the vehicle from a radiating antenna at 24, 46.8 and 77 GHz at the maximum EIRP was 0.76 W/m^2 at a distance of 3 m from the antenna, that is well below the reference exposure limit of 10 W/m^2 [55], [56].

The remaining papers [81]–[84] in Table 5 addressed extremely simplified exposure scenarios to estimate the temperature rise in 3D numerical models of the ear and the eye in the range of frequencies used in automotive radars. The excitation source was a pulsed plane wave in the air at the ICNIRP maximum power density of 10 W/m^2 [55]. Although papers [81]–[84] addressed a generic plane wave exposure

TABLE 5. Studies on EMF exposure assessment inside the car – frequencies in the 24-100 GHz region.

Study name	Frequency, power and directivity gain or type of analyzed EMF source	Study type and setup	EMF source position	Quantity measured/estimated & main study outcomes
Gustrau and Bahr [79]	77 GHz continuous wave at 1 and 10 mW/cm^2 incident power density, horn antenna.	Experimental measurement of superficial temperature increase *in vivo* (human skin) and *in vitro* (porcine eye).	Measurements are done in air with the emitting antenna close to the analyzed tissue.	Temperature rise: <0.1 ºC and 0.7 ± 0.15 ºC at 1 mW/cm^2 and 10 mW/cm^2 power density respectively.
Vermeeren *et al*. [80]	79 GHz at maximum output power (10 dBm), 2 x 2 MIMO phase modulated continuous wave radar.	Experimental measurement of the power density.	Measurements are done in air at a 3-30 mm distance above the antenna surface.	Spatial-averaged power density: the maximum value of 50 W/m^2 averaged over 1 cm^2 was observed at 3 mm distance from the antenna.
Ruddle [57]	24/46.8/77 GHz ADAS radar; plane wave.[a]	Analytical estimation through power balance methods of in-vehicle E-field strength.	External: radar antenna simulated at 3 m from car.	Power density coupled inside the vehicle cabin: among all tested sources, the highest value of 0.76 W/m^2 was obtained with the 77 GHz radar; the smallest value (0.0005 W/m^2) was with the 24 GHz radar.
Vilagosh *et al*. [81]	Pulsed excitation of 100 ps duration at 30, 60, 90 GHz, plane wave[b]	Numerical simulation using a 3D realistic anatomical model of the ear. The car is not modelled.	Plane wave in air directed towards the ear model at different incident angles.	Temperature rise in 5 s: the highest value was found at 90 GHz in the tympanic membrane, with a temperature rise of 0.00645 ºC.
Laakso *et al*. [82]	Plane wave at 6-100 GHz of 1000 J/m^2 incident energy density and pulse duration of 0.1-10 s.	Numerical simulation using a 3D anatomical model of only the eye. The car is not modelled.	Plane wave in air directed towards the eye model.	Temperature rise: the highest temperature rise was ~0.5 ºC (mean value over all the tissues and structures of the eye) at 100 GHz for pulse duration of 0.1 s. The temperature rise decreased with frequency and for longer pulse duration.
Simicevic et al. [83], [84][c]	UWB pulses at 22-29 GHz and 57-64 GHz plane wave.	Numerical simulation using 3D anatomical model of only the eye. The car is not modelled.	Plane wave in air directed towards the eye model.	Energy absorption: the energy is absorbed in the eye tissues in the same way for UWB pulses and CW excitation. At 22-29 GHz and 57-64 GHz the energy is mostly absorbed by the cornea.

[a]The devices are operated at the maximum average power density allowed at a distance of 3 m, as established in [85], that is: 0.0009 W/m^2 for 24 GHz side/rear radar; 0.3 W/m^2 for 46.8 GHz side/rear radar; 0.6 W/m^2 for 46.8 GHz ACC radar; 0.88 W/m^2 for 77 GHz side/rear/ACC radar. [b]The amplitude of the excitation signal was adjusted to the general public exposure recommendations of a maximum incident power density of 10 W/m^2 [55], [56]. [c]The papers do not specify the output power of the tested antennas.

scenario not particular to cars, we decided to include them in the current survey as they assessed the exposure generated by pulsed waveforms with the same duration and frequencies used in automotive radars. Results from these latter studies evidenced that the temperature rise was of the order of 0.5 °C, that is below the local exposure safe limit of 5 °C for Type-1 tissues and 2 °C for Type-2 tissues [55], [56].

VI. OPEN ISSUES

Despite the massive and pervasive use in modern vehicles and the resulting potential impact on the health of car occupants, we could find only a very few studies that addressed the specific scenario of EMF exposure in the connected car. The majority of past studies focused on the use of generic personal wireless communication technologies, such as mobile phones, Bluetooth and WiFi devices. Only a few studies ([57], [58], [59]) addressed technologies specific to car connectivity, such as V2V. As for car sensing, we found only studies addressing extremely simplified exposure scenarios. Finally, we could not find any study on the exposure generated by IoT sensors and actuators, specifically used in intra-vehicle wireless networks.

Research on EMF exposure in the connected car shall go deeper in the forthcoming years to address more realistic scenarios to consider aspects not yet investigated, such as:

1) The effect of the combined use of technologies operating at different frequency bands. As described in the current paper, a connected car is a kind of 'eco-system' where a variety of different wireless technologies are used at the same time, e.g., ADAS radars, antennas for V2X connectivity, intra-car wireless connectivity and infotainment that are operated at different frequency bands. Thus, a realistic assessment of RF exposure in car passengers shall take into account the peculiarity of this multi-source and multi-frequency scenario. At the moment, current studies addressed only single-frequency scenarios. Instead, in situations of simultaneous exposure to fields at different frequency bands (like in the connected car), it is important to assess the compliance with exposure limits not only in each separate frequency band but also as a whole to account for possible additive effects of multiple exposure [55], [56]. As a matter of fact, recommendations in [55], [56] provide specific formulae to assess cumulative exposure by assuming worst-case conditions (i.e., pure additive effects) among the fields from multiple sources.
2) The effect of the number of devices simultaneously used in the car. Differently from use-cases that are already extensively addressed in the literature where the exposure scenario consists of a user and a single source of EMF, e.g. in the assessment of the dose absorbed by using a smartphone or a tablet, the typical exposure scenario in the car is intrinsically a multi-source one. V2X connectivity, for example, requires multiple antennas to be mounted on the car roof or embedded in the windscreen or the external mirrors; in intra-car wireless connectivity, multiple IoT sensors and actuators are placed on different parts of the car; similarly, a typical ADAS implementation requires multiple radars mounted on the car body, e.g., on the bumpers and at the sides of the vehicle. Even by considering the simplest scenario of a single technology (i.e., a single frequency band), the exposure field inside the car varies with the number of devices as it is influenced not only by pure additive effects but also by resonance and interference effects generated by the partially closed structure of the vehicle cabin [51]–[53].
3) The effect of the variability of the exposure scenario, e.g., the effect of the size and shape of the car, the age (children vs. adults and pregnant women) and size of passengers (height, weight, body composition), the position of the devices and passengers in the car (EMF exposure depends on the distance between the source of the field and the person). For example, as to the effect of age, it is well known that the dose of EMF absorbed by a person varies with the person's age as a result not only of the different total body mass (adults are bigger and heavier than children and neonates) but also the different body composition (muscle and fat tissues have different dielectric properties and thus they absorb the field in a different way). As a matter of fact, previous studies (see, e.g., [88], [89]) observed that whole body and local SAR could have higher levels in children than adults, for identical exposure conditions. Because of the massive number of computationally demanding simulations that would be required, characterization of such variability is nearly unfeasible using deterministic dosimetry (as done by the studies in the current survey) and standard techniques of uncertainty propagation, such as Monte Carlo method [90]. Recently, advanced statistic approaches such as stochastic dosimetry and Machine Learning were applied to build computationally efficient surrogate models to assess EMF exposure in complex and uncertain scenarios [91]–[93]. It is thus recommended that future assessment of EMF exposure in the car would address uncertainty and variability of the exposure scenario with such innovative approaches.
4) In the current survey, we reported on studies addressing RF exposure of the driver/passengers in a connected car. However, it is worth mentioning that a few wireless technologies of the connected car, such V2X communication and automotive radars are expected to expose more not the car users (driver, passengers) themselves but road users in the car vicinity (pedestrians, cyclists, etc.). Although it is an important topic, this latter exposure is not yet being systematically assessed in the current literature, a part from a couple of seminal studies [94], [95] that assessed V2X exposure in road users by means of computational electromagnetic approaches.
5) Last but not least, exposure in the connected vehicle shall address the new forthcoming scenarios that will make use of innovative communication technologies such as 5G and 6G [96] at frequencies scarcely investigates up to now, e.g., mmWaves.

VII. CONCLUSION

This paper the paper summarizes results from the current literature about the characteristics and application domain of the main technologies used in the connected car, ranging from technologies for vehicle-to-everything connectivity to technologies for car sensing and intra-vehicle wireless connectivity. The paper also extensively describes the exposure field and the dose of EMF absorbed by passengers of cars equipped with such technologies, including the generic technologies for in-car personal connectivity (e.g., smartphones, tablets, etc.), as derived from current literature. All studies analyzed in the current survey evidenced that in no case the exposure field and the dose absorbed in car passengers were

above the safe limits of exposure for the general population. Nevertheless, research on EMF exposure in the connected car shall address in the forthcoming years still open challenges to address more realistic scenarios and to consider aspects not yet investigated, such as simultaneous and combined exposure to field from multiple sources at different frequencies, the effect of the variability of the exposure scenario and the impact of new 5G and 6G technologies and very high frequencies in the mmWave band on EMF exposure in the car.

REFERENCES

[1] X. Shen, R. Fantacci, and S. Chen, "Internet of Vehicles," *Proc. IEEE*, vol. 108, no. 2, pp. 242–245, Feb. 2020.

[2] G. Lasser, L. W. Mayer, and C. F. Mecklenbrauker, "Compact low profile UHF switched-beam antenna for advanced tyre monitoring systems," in *Proc. IEEE-APS Topical Conf. Antennas Propag. Wireless Commun. (APWC)*, Sep. 2012, pp. 732–735.

[3] K. Vaesen, A. Visweswaran, S. Sinha, A. Bourdoux, B. van Liempd, and P. Wambacq, "Integrated 140 GHz FMCW radar for vital sign monitoring and gesture recognition," *Microw. J.*, vol. 62, pp. 50–58, Jun. 2019. [Online]. Available: https://www.microwavejournal.com/articles/32446-integrated-140-ghz-fmcw-radar-for-vital-sign-monitoring-and-gesture-recognition

[4] A. Bazzi, G. Cecchini, M. Menarini, B. M. Masini, and A. Zanella, "Survey and perspectives of vehicular Wi-Fi versus sidelink cellular-V2X in the 5G era," *Future Internet*, vol. 11, no. 6, p. 122, May 2019.

[5] *IEEE Standard for Information technology—Local and metropolitan area networks—Specific requirements—Part 11: Wireless LAN Medium Access Control (MAC) and Physical Layer (PHY) Specifications Amendment 6: Wireless Access in Vehicular Environments*, Standard 802.11p-2010, IEEE, 2010.

[6] *Intelligent Transport Systems (ITS); Radiocommunications Equipment Operating in the 5 855 MHz to 5 925 MHz Frequency Band; Harmonised Standard Covering the Essential Requirements of Article 3.2 of Directive 2014/53/EU*, Standard ETSI EN 302 571 V2.1.1, 2017.

[7] *Intelligent Transport Systems (ITS); LTE-V2X Access Layer Specification for Intelligent Transport Systems Operating in the 5 GHz Frequency Band*, Standard ETSI EN 303 613 V1.1.1, 2020.

[8] *Technical Specification Group Radio Access Network; Study on LTE-based V2X Services; (Release 14)*, document TR 36.885 V14.0.0, 3GPP, 2016.

[9] *LTE; Evolved Universal Terrestrial Radio Access (E-UTRA); User Equipment (UE) Radio Transmission and Reception*, document ETSI TS 136 101 V14.20.0, 3GPP, TS 36.101 version 14.20.0 Release 14, 2021.

[10] *Technical Specification Group Radio Access Network; V2X Services Based on NR; User Equipment (UE) Radio Transmission and Reception; (Release 16)*, document TR 38.886 V16.3.0, 3GPP, 2021.

[11] *Technical Specification Group Radio Access Network; NR Sidelink Enhancement; User Equipment (UE) Radio Transmission and Reception; (Release 17)*, document TR 38.785 V0.5.0, 3GPP, 2022.

[12] S. Eichler, "Performance evaluation of the IEEE 802.11p WAVE communication standard," in *Proc. IEEE 66th Veh. Technol. Conf.*, Baltimore, MD, USA, Sep. 2007, pp. 2199–2203.

[13] *Transport and Traffic Telematics (TTT); Dedicated Short Range Communication (DSRC) Transmission Equipment (500 Kbit/s/250 Kbit/s) Operating in the 5 795 MHz to 5 815 MHz Frequency Band; Part 2: Harmonised Standard for Access to Radio Spectrum; Sub—Part 2: On-Board Units (OBU)*, Standard ETSI EN 300 674-2-2 V2.2.1, 2019.

[14] *Electromagnetic Compatibility and Radio Spectrum Matters (ERM); Short Range Devices; Radio Equipment to be Used in the 1 GHz to 40 GHz Frequency Range; Part 1: Technical Characteristics and Test Methods*, Standard ETSI EN 300 440-1 V1.6.1, 2010.

[15] *Electromagnetic Compatibility and Radio Spectrum Matters (ERM); Short Range Devices; Road Transport and Traffic Telematics (RTTT); Short Range Radar Equipment Operating in the 24 GHz Range; Part 1: Technical Requirements and Methods of Measurement*, Standard ETSI EN 302 288-1 V1.6.1, 2012.

[16] *Short Range Devices; Transport and Traffic Telematics (TTT); Radar Equipment operating in the 76 GHz to 77 GHz range; Harmonised Standard Covering the Essential Requirements of Article 3.2 of Directive 2014/53/EU; Part 1: Ground Based Vehicular Radar*, Standard ETSI EN 301 091-1 V2.1.1, 2017.

[17] *Electromagnetic Compatibility and Radio Spectrum Matters (ERM); Short Range Devices; Road Transport and Traffic Telematics (RTTT); Short Range Radar Equipment Operating in the 77 GHz to 81 GHz Band; Part 1: Technical Requirements and Methods of Measurement*, Standard ETSI EN 302 264-1 V1.1.1, 2009.

[18] H. Abedi, S. Luo, V. Mazumdar, M. M. Y. R. Riad, and G. Shaker, "AI-powered in-vehicle passenger monitoring using low-cost mm-wave radar," *IEEE Access*, vol. 10, pp. 18998–19012, 2022.

[19] (2020). Texas Instruments. *Design Guide: TIDEP-01023 Child-Presence and Occupant-Detection Reference Design Using 60-GHz Antenna-on-Package mmWave Sensor*. [Online]. Available: https://www.ti.com/lit/pdf/TIDUEY3

[20] (2020). Texas Instrument. *Design Guide: TIDEP-01001 Vehicle Occupant Detection Reference Design*. [Online]. Available: https://www.ti.com/lit/pdf/TIDUE95A

[21] (2021). *Bitsensing, 60GHz MOD620*. [Online]. Available: https://bitsensing.com/60ghz-mod620/

[22] (2021). Novelic. *Automotive in-Cabin Monitoring*. [Online]. Available: https://www.novelic.com/wp-content/uploads/2021/02/NIC_MBT_ACAM_v5.0.pdf

[23] Innosent. *Incabin Radar Monitoring*. Accessed: Mar. 2022. [Online]. Available: https://www.innosent.de/en/automotive/incabin-radar-monitoring/

[24] (2020). Vayyar. *Vayyar Element Development Module*. [Online]. Available: https://vayyar.s3.eu-central-1.amazonaws.com/PDF/Vayyar+Element+Development+Module+-+Hardware+Specs.pdf

[25] (2021). Infineon. *Automotive 60 GHz Radar Application Kit*. [Online]. Available: https://www.infineon.com/dgdl/Infineon-Automotive_60_GHz_radar_application_kit-ProductBrief-v01_00-EN.pdf?fileId=5546d46277921c320177b11d0d1757ad

[26] (2021). NXP. *In-Cabin UWB Radar NXPLive Demo*. [Online]. Available: https://www.nxp.com/video/in-cabin-uwb-radar-nxplive-demo: CES-2021-IN-CABIN-UWB-RADAR-VIDEO

[27] M. Koca, G. Gurbilek, B. Soner, and S. Coleri, "Empirical feasibility analysis for energy harvesting intravehicular wireless sensor networks," *IEEE Internet Things J.*, vol. 8, no. 1, pp. 179–186, Jan. 2021.

[28] Y. Huo, W. Tu, Z. Sheng, and V. C. M. Leung, "A survey of in-vehicle communications: Requirements, solutions and opportunities in IoT," in *Proc. IEEE 2nd World Forum Internet Things (WF-IoT)*, Dec. 2015, pp. 132–137.

[29] N. Lu, N. Cheng, N. Zhang, X. Shen, and J. W. Mark, "Connected vehicles: Solutions and challenges," *IEEE Internet Things J.*, vol. 1, no. 4, pp. 289–299, Aug. 2014.

[30] P. López-Iturri, E. Aguirre, L. Azpilicueta, U. Garate, and F. Falcone, "ZigBee radio channel analysis in a complex vehicular environment [wireless corner]," *IEEE Antennas Propag. Mag.*, vol. 56, no. 4, pp. 232–245, Aug. 2014.

[31] D. Balachander and T. R. Rao, "In-vehicle RF propagation measurements for electronic infotainment applications at 433/868/915/2400 MHz," in *Proc. Int. Conf. Adv. Comput., Commun. Informat. (ICACCI)*, Aug. 2013, pp. 1408–1413.

[32] T. R. Rao, D. Balachander, P. Sathish, and N. Tiwari, "Intra-vehicular RF propagation measurements at UHF for wireless sensor networks," in *Proc. Int. Conf. Recent Adv. Comput. Softw. Syst.*, Apr. 2012, pp. 214–218.

[33] O. K. Tonguz, H.-M. Tsai, C. Saraydar, T. Talty, and A. Macdonald, "Intra-car wireless sensor networks using RFID: Opportunities and challenges," in *Proc. Mobile Netw. Veh. Environ.*, May 2007, pp. 43–48.

[34] T. Nolte, H. Hansson, and L. lo Bello, "Automotive communications–past, current and future," in *Proc. IEEE Conf. Emerg. Technol. Factory Autom.*, Catania, Italy, 2005, pp. 985–992.

[35] M. Heddebaut, V. Deniau, and K. Adouane, "In-vehicle WLAN radio-frequency communication characterization," *IEEE Trans. Intell. Transp. Syst.*, vol. 5, no. 2, pp. 114–121, Jun. 2004.

[36] *IEEE Standard for Information Technology—Local and Metropolitan area Networks—Specific Requirements– -Part 15.1A: Wireless Medium Access Control (MAC) and Physical Layer (PHY) Specifications for Wireless Personal Area Networks (WPAN)*, Standard 802.15.1-2005, IEEE, 2005.

[37] *Wideband Transmission Systems; Data Transmission Equipment Operating in the 2,4 GHz Band; Harmonised Standard for Access to Radio Spectrum*, Standard ETSI EN 300 328 V2.2.2, 2019.

[38] *Short Range Devices (SRD); Radio Equipment to be Used in the 1 GHz to 40 GHz Frequency Range; Harmonised Standard for Access to Radio Spectrum*, Standard ETSI EN 300 440 V2.2.1, 2018.

[39] *ElectroMagnetic Compatibility (EMC) Standard for Radio Equipment and Services; Part 17: Specific Conditions for Broadband Data Transmission Systems; Harmonised Standard for ElectroMagnetic Compatibility*, Standard ETSI EN 301 489-17 V3.2.4, 2020.

[40] *Bluetooth Core Specification Version 5.3*, Bluetooth SIG, Kirkland, Brentwood, Tennessee, USA, 2021.

[41] *Electromagnetic Compatibility and Radio Spectrum Matters (ERM); Technical Characteristics of Short Range Devices (SRD) and RFID in the UHF Band; System Reference Document for Radio Frequency Identification (RFID) and SRD Equipment; Part 2: Additional Spectrum Requirements for UHF RFID, Non-Specific SRDs and Specific SRDs*, Standard ETSI TR 102 649-2 V1.3.1, 2012.

[42] *Short Range Devices (SRD) Operating in the Frequency Range 25 MHz to 1 000 MHz; Part 1: Technical Characteristics and Methods of Measurement*, Standard ETSI EN 300 220-1 V3.1.1, 2017.

[43] *Short Range Devices (SRD) Operating in the Frequency Range 25 MHz to 1 000 MHz; Part 2: Harmonised Standard for Access to Radio Spectrum for Non Specific Radio Equipment*, Standard ETSI EN 300 220-2 V3.2.1, 2018.

[44] *ERC Recommendation Relating to the use of Short Range Devices (SRD), ERC Recommendation 70–03*, Electron. Commun. Committee, Copenhagen, Denmark 2021.

[45] *Code of Federal Regulations (CFR), Title 47-Telecommunication, Part 15-Radio Frequency Devices, 47 CFR Part 15*, Federal Government, Washington, DC, USA, 2022.

[46] *Code of Federal Regulations (CFR), Title 47-Telecommunication, Part 15-Radio Frequency Devices, Subpart F-Ultra-Wideband Operation, 47 CFR Part 15 Subpart F*, Federal Government, Washington, DC, USA, 2022.

[47] *Short Range Devices (SRD) Using Ultra Wide Band technology (UWB); Harmonised Standard Covering the Essential Requirements of Article 3.2 of the Directive 2014/53/EU; Part 3: Requirements for UWB Devices for Ground Based Vehicular Applications*, Standard ETSI EN 302 065-3 V2.1.1, 2016.

[48] *IEEE Standard for Low-Rate Wireless Networks—Amendment 1: Enhanced Ultra Wideband (UWB) Physical Layers (PHYs) and Associated Ranging Techniques*, Standard 802.15.4z-2020, IEEE, 2020.

[49] *Information Technology—Radio Frequency Identification for Item Management—Part 3: Parameters for air Interface Communications at 13,56 MHz*, Standard ISO/IEC 18000-3:2010, 2010.

[50] *Short Range Devices (SRD); Radio Equipment in the Frequency Range 9 kHz to 25 MHz and Inductive Loop Systems in the Frequency Range 9 kHz to 30 MHz; Harmonised Standard Covering the Essential Requirements of Article 3.2 of Directive 2014/53/EU*, Standard ETSI EN 300 330 V2.1.1, 2017.

[51] A. Hirata and T. Ida, "Analysis of electromagnetic environment in a CAD-based vehicle with a human body for far-field incidence," *IEEE Antennas Wireless Propag. Lett.*, vol. 7, pp. 625–628, 2008.

[52] A. Hirata, "Computational electromagnetic dosimetry of a human body in a vehicle for plane-wave exposure," *IEEJ Trans. Fundamentals Mater.*, vol. 129, no. 10, pp. 725–726, 2009.

[53] L. Low, A. R. Ruddle, J. M. Rigelsford, and R. J. Langley, "Computed impact of human occupants on field distributions within a passenger vehicle," in *Proc. 6th Eur. Conf. Antennas Propag. (EUCAP)*, Prague, Czech Republic, Mar. 2012, pp. 1214–1217.

[54] E. Tanghe, W. Joseph, L. Verloock, and L. Martens, "Evaluation of vehicle penetration loss at wireless communication frequencies," *IEEE Trans. Veh. Technol.*, vol. 57, no. 4, pp. 2036–2041, Jul. 2008.

[55] G. Ziegelberger, R. Croft, M. Feychting, A. C. Green, A. Hirata, G. d'Inzeo, K. Jokela, S. Loughran, C. Marino, S. Miller, and G. Oftedal, "ICNIRP guidelines for limiting exposure to electromagnetic fields (100 kHz to 300 GHz)," *Health Phys.*, vol. 118, pp. 483–524, May 2020.

[56] *IEEE Standard for Safety Levels with Respect to Human Exposure to Electric, Magnetic, and Electromagnetic Fields, 0 Hz to 300 GHz*, Standard C95.1-2019, IEEE, Oct. 2019, pp. 1–312.

[57] A. R. Ruddle, "Preliminary estimates of electromagnetic field exposures due to advanced vehicle technologies," in *Proc. Loughborough Antennas Propag. Conf. (LAPC)*, Loughborough, U.K., Nov. 2016, pp. 1–5.

[58] G. Tognola, B. Masini, S. Gallucci, M. Bonato, S. Fiocchi, E. Chiaramello, M. Parazzini, and P. Ravazzani, "Numerical assessment of RF human exposure in smart mobility communications," *IEEE J. Electromagn., RF Microw. Med. Biol.*, vol. 5, no. 2, pp. 100–107, Jun. 2021.

[59] G. Tognola, B. Masini, S. Gallucci, M. Bonato, S. Fiocchi, E. Chiaramello, L. Dossi, M. Parazzini, and P. Ravazzani, "Smart mobility communication and human exposure to RF fields: A numerical dosimetry approach," in *Proc. 23rd Gen. Assem. Sci. Symp. Int. Union Radio Sci.*, Rome, Italy, Aug. 2020, pp. 1–4.

[60] E. Baramili, R. Sarkis, and M. B. Saleh, "Investigation of driver EMF exposure from 4G/5G automotive glass mounted antennas," in *Proc. IEEE Int. Symp. Antennas Propag. North Amer. Radio Sci. Meeting*, Montreal, QC, Canada, Jul. 2020, pp. 1451–1452.

[61] Y. Tarusawa, S. Nishiki, and T. Nojima, "Fine positioning three-dimensional electric-field measurements in automotive environments," *IEEE Trans. Veh. Technol.*, vol. 56, no. 3, pp. 1295–1306, May 2007.

[62] A. R. Ruddle, L. Low, J. M. Rigelsford, and R. J. Langley, "Variation of computed in-vehicle SAR with number and location of occupants at commonly used communications frequencies," in *Proc. 10th Int. Symp. Electromagn. Compat.*, York, U.K., 2011, pp. 756–761.

[63] D. O. McCoy, D. M. Zakharia, and Q. Balzano, "Field strengths and specific absorption rates in automotive environments," *IEEE Trans. Veh. Technol.*, vol. 48, no. 4, pp. 1287–1303, Jul. 1999.

[64] G. Anzaldi, "Validation procedure for final users applied to automotive environments," in *Proc. IEE Validation Comput. Electromagn. Seminar*, Manchester, U.K., 2004, pp. 43–47.

[65] R. A. A. Rodrigues, G. Fontgalland, G. F. Aragão, and F. C. L. Federal, "Measurement with quasi-isotropic antenna of CEM coming from multi-source in a reverberation chamber and in a car," *J. Microw., Optoelectron. Electromagn. Appl.*, vol. 12, no. 2, pp. 466–483, Dec. 2013.

[66] R. Buckus, B. Strukcinskiene, and J. Raistenskis, "The assessment of electromagnetic field radiation exposure for mobile phone users," *Vojnosanitetski pregled*, vol. 71, no. 12, pp. 1138–1143, 2014.

[67] Z. Psenakova, D. Gombarska, and M. Smetana, "Electromagnetic field measurement inside the car with modern embedded wireless technologies," in *Proc. IEEE 21st Int. Conf. Comput. Problems Electr. Eng. (CPEE)*, Poland, Sep. 2020, pp. 1–4.

[68] E. Aguirre, P. L. Iturri, L. Azpilicueta, S. de Miguel-Bilbao, V. Ramos, U. Gárate, and F. Falcone, "Analysis of estimation of electromagnetic dosimetric values from non-ionizing radiofrequency fields in conventional road vehicle environments," *Electromagn. Biol. Med.*, vol. 34, no. 1, pp. 19–28, 2015.

[69] L. Low and A. R. Ruddle, "Vehicle interaction with electromagnetic fields and implications for intelligent transport systems (ITS) development," in *Intelligent Transport Systems: Technologies and Applications*, A. Perallos, U. Hernandez-Jayo, E. Onieva, I. J. García-Zuazola, Eds. Chichester, U.K.: Wiley, 2016, pp. 107–130.

[70] A. Toropainen, "Human exposure by mobile phones in enclosed areas," *Bioelectromagnetics*, vol. 24, no. 1, pp. 63–65, Jan. 2003.

[71] S. Lee, J. Lee, S. Yoon, and J. Choi, "Relationship between electric field exposure and whole-body averaged SAR in automotive environments," in *Proc. 10th Eur. Conf. Antennas Propag. (EuCAP)*, Davos, Switzerland, Apr. 2016, pp. 1–3.

[72] G. Anzaldi, F. Silva, M. Fernandez, M. Quilez, and P. J. Riu, "Initial analysis of SAR from a cell phone inside a vehicle by numerical computation," *IEEE Trans. Biomed. Eng.*, vol. 54, no. 5, pp. 921–930, May 2007.

[73] K. H. Chan, S. W. Leung, and Y. M. Siu, "Specific absorption rate evaluation for people using wireless communication device in vehicle," in *Proc. IEEE Int. Symp. Electromagn. Compat.*, Fort Lauderdale, FL, USA, Jul. 2010, pp. 706–711.

[74] S.-W. Leung, Y. Diao, K.-H. Chan, Y.-M. Siu, and Y. Wu, "Specific absorption rate evaluation for passengers using wireless communication devices inside vehicles with different handedness, passenger counts, and seating locations," *IEEE Trans. Biomed. Eng.*, vol. 59, no. 10, pp. 2905–2912, Oct. 2012.

[75] Y. Diao, W. N. Sun, K. H. Chan, S. W. Leung, and Y. M. Siu, "SAR evaluation for multiple wireless communication devices inside a vehicle," in *Proc. Int. Symp. Electromagn. Theory*, Hiroshima, Japan, May 2013, pp. 626–629.

[76] L.-R. Harris, M. Zhadobov, N. Chahat, and R. Sauleau, "Electromagnetic dosimetry for adult and child models within a car: Multi-exposure scenarios," *Int. J. Microw. Wireless Technol.*, vol. 3, no. 6, pp. 707–715, Dec. 2011.

[77] V. B. Jeladze, T. R. Nozadze, V. A. Tabatadze, I. A. Petoev-Darsavelidze, M. M. Prishvin, and R. S. Zaridze, "Electromagnetic exposure study on a human located inside the car using the method of auxiliary sources," *J. Commun. Technol. Electron.*, vol. 65, no. 5, pp. 457–464, May 2020.
[78] R. Aminzadeh, A. Abdolali, and H. Khaligh, "A numerical study on the interaction between different position of cellular headsets and a human head," *ACES J.*, vol. 29, pp. 91–98, Jan. 2014.
[79] F. Gustrau and A. Bahr, "W-band investigation of material parameters, SAR distribution, and thermal response in human tissue," *IEEE Trans. Microw. Theory Techn.*, vol. 50, no. 10, pp. 2393–2400, Oct. 2002.
[80] G. Vermeeren, S. Kuehn, B. Debaillie, G. Torfs, N. Kuster, P. Demeester, W. Van Thillo, L. Martens, and W. Joseph, "Exposure assessment of 60 GHz communication antenna and 79 GHz automotive radar," in *Proc. Joint Annu. Meeting Bioelectromagnetics Soc. Eur. BioElectromagnetics Assoc.*, Piran, Portorož, Slovenia, 2018, pp. 222–225.
[81] Z. Vilagosh, A. Lajevardipour, and A. Wood, "Computer simulation study of the penetration of pulsed 30, 60 and 90 GHz radiation into the human ear," *Sci. Rep.*, vol. 10, no. 1, pp. 1–10, Dec. 2020.
[82] I. Laakso, R. Morimoto, J. Heinonen, K. Jokela, and A. Hirata, "Human exposure to pulsed fields in the frequency range from 6 to 100 GHz," *Phys. Med. Biol.*, vol. 62, no. 17, pp. 6980–6992, Aug. 2017.
[83] N. Simicevic, "FDTD computation of human eye exposure to ultra-wideband electromagnetic pulses," *Phys. Med. Biol.*, vol. 53, no. 6, pp. 1795–1809, Mar. 2008.
[84] N. Simicevic, "Dosimetric implication of exposure of human eye to ultra-wideband electromagnetic pulses," in *Proc. Asia–Pacific Symp. Electromagn. Compat. 19th Int. Zurich Symp. Electromagn. Compat.*, Singapore, May 2008, pp. 208–211.
[85] *Amendment of Sections 15.35 and 15.253 of the Commission's Rules Regarding Operation of Radar Systems in the 76-77 GHz Band and Amendment of Section 15.253 of the Commission's Rules to Permit Fixed use of Radar in the 76-77 GHz Band*, document FCC 12–72, 2012.
[86] D. A. Hill, M. T. Ma, A. R. Ondrejka, B. F. Riddle, M. L. Crawford, and R. T. Johnk, "Aperture excitation of electrically large, lossy cavities," *IEEE Trans. Electromagn. Compat.*, vol. 36, no. 3, pp. 169–178, Aug. 1994.
[87] K. Yee, "Numerical solution of initial boundary value problems involving Maxwell's equations in isotropic media," *IEEE Trans. Antennas Propag.*, vol. AP-14, no. 3, pp. 302–307, May 1966.
[88] J. Wiart, A. Hadjem, M. F. Wong, and I. Bloch, "Analysis of RF exposure in the head tissues of children and adults," *Phys. Med. Biol.*, vol. 53, no. 13, pp. 3681–3695, Jul. 2008.
[89] A. Christ, M.-C. Gosselin, M. Christopoulou, S. Kühn, and N. Kuster, "Age-dependent tissue-specific exposure of cell phone users," *Phys. Med. Biol.*, vol. 55, no. 7, pp. 1767–1783, Apr. 2010.
[90] B. Sudret, S. Marelli, and J. Wiart, "Surrogate models for uncertainty quantification: An overview," in *Proc. 11th Eur. Conf. Antennas Propag. (EUCAP)*, Paris, France, Mar. 2017, pp. 793–797.
[91] M. Bonato, L. Dossi, E. Chiaramello, S. Fiocchi, G. Tognola, and M. Parazzini, "Stochastic dosimetry assessment of the human RF-EMF exposure to 3D beamforming antennas in indoor 5G networks," *Appl. Sci. (Switzerland)*, vol. 11(4), art. no. 1751, pp. 1–14, 2021.
[92] G. Tognola, D. Plets, E. Chiaramello, S. Gallucci, M. Bonato, S. Fiocchi, M. Parazzini, L. Martens, W. Joseph, and P. Ravazzani, "Use of machine learning for the estimation of down- and up-link field exposure in multi-source indoor WiFi scenarios," *Bioelectromagnetics*, vol. 42, no. 7, pp. 550–561, Oct. 2021.
[93] G. Tognola, M. Bonato, E. Chiaramello, S. Fiocchi, I. Magne, M. Souques, M. Parazzini, and P. Ravazzani, "Use of machine learning in the analysis of indoor ELF MF exposure in children," *Int. J. Environ. Res. Public Health*, vol. 16, no. 7, p. 1230, Apr. 2019.
[94] M. Benini, M. Bonato, S. Gallucci, E. Chiaramello, S. Fiocchi, M. Parazzini, and G. Tognola, "Assessment of road-user exposure from ITS-5.9 GHz vehicular connectivity technology," in *Proc. Annu. Meeting BIOEM Soc.*, Nagoya, Japan, 2022.
[95] M. Bonato, M. Benini, S. Gallucci, E. Chiaramello, S. Fiocchi, M. Parazzini, and G. Tognola, "Assessment of EMF exposure in 5G connected vehicles," in *Proc. Annu. Meeting BIOEM Soc.*, Nagoya, Japan, 2022.
[96] M. Mizmizi, F. Linsalata, M. Brambilla, F. Morandi, K. Dong, M. Magarini, M. Nicoli, M. N. Khormuji, P. Wang, R. A. Pitaval, and U. Spagnolini, "Fastening the initial access in 5G NR sidelink for 6G V2X networks," *Veh. Commun.*, vol. 33, Jan. 2022, Art. no. 100402.

GABRIELLA TOGNOLA received the master's degree in electronic engineering and the Ph.D. degree in bioengineering from the Politecnico di Milano, Milan, Italy. She is currently a Senior Research Scientist with the Institute of Electronics, Computer and Telecommunication Engineering, Consiglio Nazionale delle Ricerche. Her research interests include exposure assessment of electromagnetic fields with numerical dosimetry and with machine learning methods and modeling of electromagnetic fields for biomedical applications and innovative EMF applications in the connected vehicle.

MARTA BONATO (Student Member, IEEE) received the master's degree in biomedical engineering and the Ph.D. degree in bioengineering from the Polytechnic of Milan, Milan, Italy, in 2017 and 2021, respectively. Since September 2017, she has been with the Institute of Electronics, Computer, and Telecommunication Engineering, Consiglio Nazionale delle Ricerche, Rome, Italy, as a Research Fellow. Her research interests include the study of the interaction of electromagnetic fields (EMF) with biological systems and the study of possible effects of EMF on health with both deterministic and stochastic dosimetry.

MARTINA BENINI received the B.S. degree in biomedical engineering from Alma Mater Studiorum—Università di Bologna, Italy, in 2017, and the M.S. degree in biomedical engineering from the Politecnico di Milano, Italy, in 2020, where she is currently pursuing the Ph.D. degree in bioengineering. From October 2020 to April 2021, she was a Research Fellow with the Institute of Electronics, Information Engineering and Telecommunications (IEIIT), Consiglio Nazionale delle Ricerce (CNR). Her research interests include the study of the interaction between the electromagnetic fields (EMFs) and the human body with both deterministic and stochastic dosimetry, with a focus on the antennas used in the automotive field for vehicular connectivity.

SAM AERTS was born in Sint-Niklaas, Belgium, in 1988. He received the M.Sc. degree in applied physics and the Ph.D. degree in electrical engineering from Ghent University, Ghent, Belgium, in 2011 and 2017, respectively. Since 2017, he has been a Postdoctoral Fellow with the Research Foundation—Flanders (FWO), Belgium, with the WAVES Research Group, IMEC, UGent.

SILVIA GALLUCCI received the master's degree in biomedical engineering from the University of Pisa, Pisa, Italy, in 2019. She is currently pursuing the Ph.D. degree in bioengineering with the Politecnico di Milano, Milan, Italy, for studying the EMF–human interactions. From 2019 to 2020, she was a Research Fellow with the Institute of Electronics, Computer, and Telecommunication Engineering, Consiglio Nazionale delle Ricerche, Rome, Italy. Her research interests include the exposure assessment of electromagnetic fields with numerical dosimetry, particularly from 5G mobile communications.

EMMA CHIARAMELLO (Member, IEEE) received the master's and Ph.D. degrees in biomedical engineering from the Politecnico di Torino, Torino, Italy, in 2009 and 2013, respectively. She is currently a Research Scientist with the Institute of Electronics, Computer, and Telecommunication Engineering, National Research Council of Italy, Rome, Italy. Her research interests include the study of the interactions between EMF and biological systems, with both deterministic dosimetry based on computational electromagnetism methods and stochastic dosimetry based on surrogate modeling.

SERENA FIOCCHI received the master's degree in biomedical engineering and the Ph.D. degree in bioengineering from the Polytechnic University of Milan, Milan, Italy, in 2009 and 2014, respectively. She is currently a Research Scientist with the Institute of Electronics, Computer, and Telecommunication Engineering, National Research Council of Italy, Rome, Italy. Her research interests include the study of the computational modeling of noninvasive brain and spinal stimulation techniques, the design and the optimization of biomedical technologies based on electromagnetic fields (EMF) for diagnostic and therapeutic applications, and the computational modeling of the interactions between EMF and biological systems.

MARTA PARAZZINI (Member, IEEE) is currently a Research Scientist with the Institute of Electronics, Computer, and Telecommunication Engineering, Italian National Research Council, Rome, Italy. Her research interests include the study of the interactions of EMF with biological systems, deterministic and stochastic computational dosimetry, and the medical applications of EMF, in particular the techniques for noninvasive brain stimulation.

BARBARA M. MASINI (Senior Member, IEEE) received the Laurea degree *(summa cum laude)* in telecommunications engineering and the Ph.D. degree in electronic, computer science, and telecommunication engineering from the University of Bologna, Italy, in 2001 and 2005, respectively. She is currently a Senior Researcher with the National Research Council (CNR) of Italy, Institute for Electronics and for Information and Telecommunications Engineering (IEIIT). She is also an Adjunct Professor with the University of Bologna. She works in the area of wireless communication systems and her research interests include connected vehicles, from physical and MAC levels aspects up to applications and field trial implementations. She received the best paper awards for research in the vehicular communications at IEEE ITST Conference, in 2017. She gave tutorials on V2X topics at ISWCS 2017 and WCNC 2019 and she served as an invited speaker in several international events. She is an Editor of IEEE Access and *Computer Communication* and she is responsible for a number of national and international projects on vehicular communications.

WOUT JOSEPH (Senior Member, IEEE) was born in Ostend, Belgium, in October 1977. He received the M.Sc. degree in electrical engineering from Ghent University, Belgium, in July 2000, and the Ph.D. degree, in March 2005, this work dealt with measuring and modeling of electromagnetic fields around base stations for mobile communications related to the health effects of the exposure to electromagnetic radiation. He was a Postdoctoral Fellow of the FWO-V (Research Foundation—Flanders), from 2007 to 2012. Since October 2009, he has been a Professor in the domain of "Experimental characterization of wireless communication systems." He has been an IMEC PI, since 2017. His research interests include electromagnetic field exposure assessment, propagation for wireless communication systems, antennas, and calibration. Furthermore, he specializes in wireless performance analysis and quality of experience.

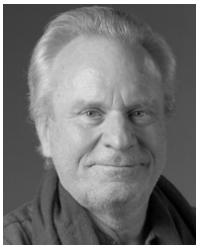

JOE WIART (Senior Member, IEEE) received the Ph.D. degree, in 1995, and the H.D.R. degree, in 2015. He was an Ingenieur General des Mines. Since 2015, he has been the Holder of the Chair C2M "Characterization, Modeling and Master of the Institut Mines Telecom" at Telecom Paris, Institut Polytechnique de Paris. He is also the Chairperson of the TC106x of the CENELEC in-charge of EMF exposure standards. He has been the Chair of URSI Commission K (electromagnetic fields and biological systems), between 2014 and 2021. His research interests include experimental, numerical methods, machine learning, artificial intelligence, and statistic applied in electromagnetism and dosimetry. His works gave rise to more than 150 publications in journal articles and more than 200 communications.

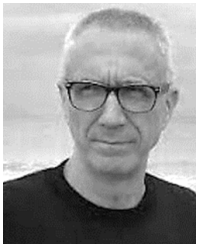

PAOLO RAVAZZANI (Member, IEEE) received the master's degree in electronic engineering and the Ph.D. degree in bioengineering from the Politecnico di Milano, Milan, Italy. He is currently the Director of Research with the Institute of Electronics, Computer, and Telecommunication Engineering, Consiglio Nazionale delle Ricerche, Rome, Italy. His research interests include the exposure assessment of electromagnetic fields related to the study of the possible effects of electromagnetic fields on health and the biomedical applications of electromagnetic fields.